ARTICLE IN PRESS

ELSEVIER

Tectonophysics 6762 (2002) xxx–xxx

TECTONOPHYSICS

www.elsevier.com/locate/tecto

The eGf method for dissimilar focal mechanisms: the Athens 1999 earthquake

Vladimir Plicka, Jiri Zahradnik*

Faculty of Mathematics and Physics, Charles University, Prague 121 16, Czech Republic

Received 21 May 2002; accepted 16 August 2002

Abstract

The empirical Green's function method (eGf) is innovated to examine the rupture nucleation and propagation during the disastrous Athens earthquake of September 7, 1999 ($M_L = 5.4$). Waveforms recorded at seven regional broadband stations are studied. One of the two strongest aftershocks ($M_L = 4$) was selected as the eGf, but its focal mechanism differs from the mainshock mechanism. Therefore, the paper suggests an innovation of the classical eGf method. The assumption of the similarity of the mainshock and aftershock focal mechanisms is relaxed as follows: the mainshock is modeled by an eGf-like method using synthetic weak events, computed by discrete wave number method (DW), two times, once with the focal mechanism of the mainshock and again with the assumed focal mechanism of the aftershock. These computations are used to determine the subset of the stations at which the disparate focal mechanism results in a (station-dependent) multiplicative factor only, with minimum waveform distortion. Real data from that station subset are then inverted as if the mainshock and aftershock mechanisms were the same. The eGf synthetics are produced for constant-velocity radial rupture propagation starting at 36 trial grid points, regularly distributed on the fault plane, and the grid point providing the best fit to the observed waveforms is assumed to be the nucleation point. Synthetic tests show that success of the method strongly depends on the exact knowledge of the mainshock true fault-plane orientation, but that is fairly well known from the aftershocks distribution in this case. The aftershock sequence suggests two possible sizes of the fault: a large fault (20 × 16 km along strike and dip, respectively) and a small fault (8 × 10 km) that fills in the gap identified during the first 12 observation days between two aftershock clusters. The eGf modeling does not resolve a preferred fault dimension. However, for both sizes, the method locates the nucleation point at the western part of the fault plane, thus clearly indicating the rupture propagation toward Athens.

Keywords: Empirical Green's function; Focal mechanism; Rupture nucleation; Athens earthquake

1. Introduction

Investigation of the earthquake source represents one of the most complex problems in seismology. Teleseismic, regional and local data should be combined as much as possible. This paper is based on the regional data.

Earthquake source inversions require a good knowledge of the medium along the source-station propagation path. The application of weak earthquakes as empirical Green's function, eGf, can overcome this limitation (Hartzell, 1978; Irikura and

* Corresponding author.
E-mail address: vladimir.plicka@mff.cuni.cz (J. Zahradnik).

0040-1951/02/$ - see front matter © 2002 Published by Elsevier Science B.V.
PII: S0040-1951(02)00440-7

Kamae, 1994; Diagourtas et al., 1994; Dreger, 1994; Frankel, 1995; Hutchings et al., 1997; Plicka and Zahradnik, 1998; Hough, 2001).

In this study, we use the eGf method to investigate the rupture nucleation and propagation. The selected aftershock and mainshock have different focal mechanisms and violate the main applicability condition of the classical eGf method. The main innovation of this work is to show that synthetic modeling is able to distinguish the stations at which eGf method can be applied even with such an "incorrect" eGf event, at least for limited time window.

The method is applied to the catastrophic earthquake of $M_L = 5.4$ which occurred on September 7, 1999, in Athens, the capital of Greece. The maximum macroseismic intensity was XIII–IX in the NW outskirts of the city where 143 people were killed and more than 2000 were injured (Stavrakakis et al., 2000; Papadimitriou et al., 2000; Tselentis and Zahradnik, 2000; Papanastassiou et al., 2000; Papadopoulos et al., 2000). This earthquake is the first known event of magnitude larger than 5 to occur so close to Athens, and thus deserves a particular attention.

2. Data

The mainshock location parameters obtained from regional network (National Observatory of Athens, NOA) and from global data (USGS) are summarized in Table 1. The epicenter of selected aftershock, $M_L = 4.0$, September 8, 1999, 12:55 GMT (Lat. = 38.14N, Lon. = 23.74E, NOA) is at about 15 km from the mainshock (NOA location). Two fault-plane solutions are known for this aftershock. One solution (strike = 220°, dip = 40°, rake = 120°) was retrieved from the amplitude spectra and polarities (Zahradnik, 2001). The other solution was obtained from the first motion polarities, only (strike = 330°, dip = 70°, rake = – 30°) by Papadopoulos et al. (2000). Both mechanisms are different from the focal mechanism of the mainshock (strike = 123°, dip = 55°, rake = – 84°, USGS).

We used the velocity time histories of the mainshock and aftershock recorded by the NOA and supplemented them by a broadband station Sergoula (SER), jointly operated by the Charles University in Prague and the University of Patras (Fig. 1). The NOA stations are equipped with Lennartz LE-3D/20s sensors. Although the sensors are three-component, the multiplexed data available from NOA contain only horizontal broadband components, while most of the vertical components come from short-period Teledyne S-13 sensors. The SER station is a three-component Guralp CMG-3T sensor. Due to breaks in some NOA data, we used only selected stations (Table 2) and E–W components.

The Athens earthquake was followed by numerous aftershocks recorded by a temporary network of 30 stations installed a few days after mainshock by the Patras University (Tselentis and Zahradnik, 2000). The network provided accurate locations that were used to estimate two possible fault rupture dimensions (20 × 16 and 8 × 10 km) (see Fig. 2A). We concentrated on the first 12 observation days, only because, later, the seismicity became more diffuse. Since the aftershock distribution was very close to one of the USGS nodal planes, we fix the fault plane in the present paper to have the USGS strike = 123° and dip = 55°.

3. Method

The classical eGf method can be applied only when the focal mechanisms of the weak event and main-

Table 1
Focal parameters of the Athens mainshock by various agencies

	Latitude (deg N)	Longitude (deg E)	Depth (km)	Moment (N m)	Strike (deg)	Dip (deg)	Rake (deg)
NOA	38.15	23.62	30	–	113	39	– 90
USGS	38.13	23.55	9	7.8×10^{17}	123	55	– 84
Harvard	38.02	23.71	15	1.2×10^{18}	114	45	– 73

NOA = National Observatory of Athens, USGS = U.S. Geological Survey, Harvard = Harvard Centroid Moment Catalogue.

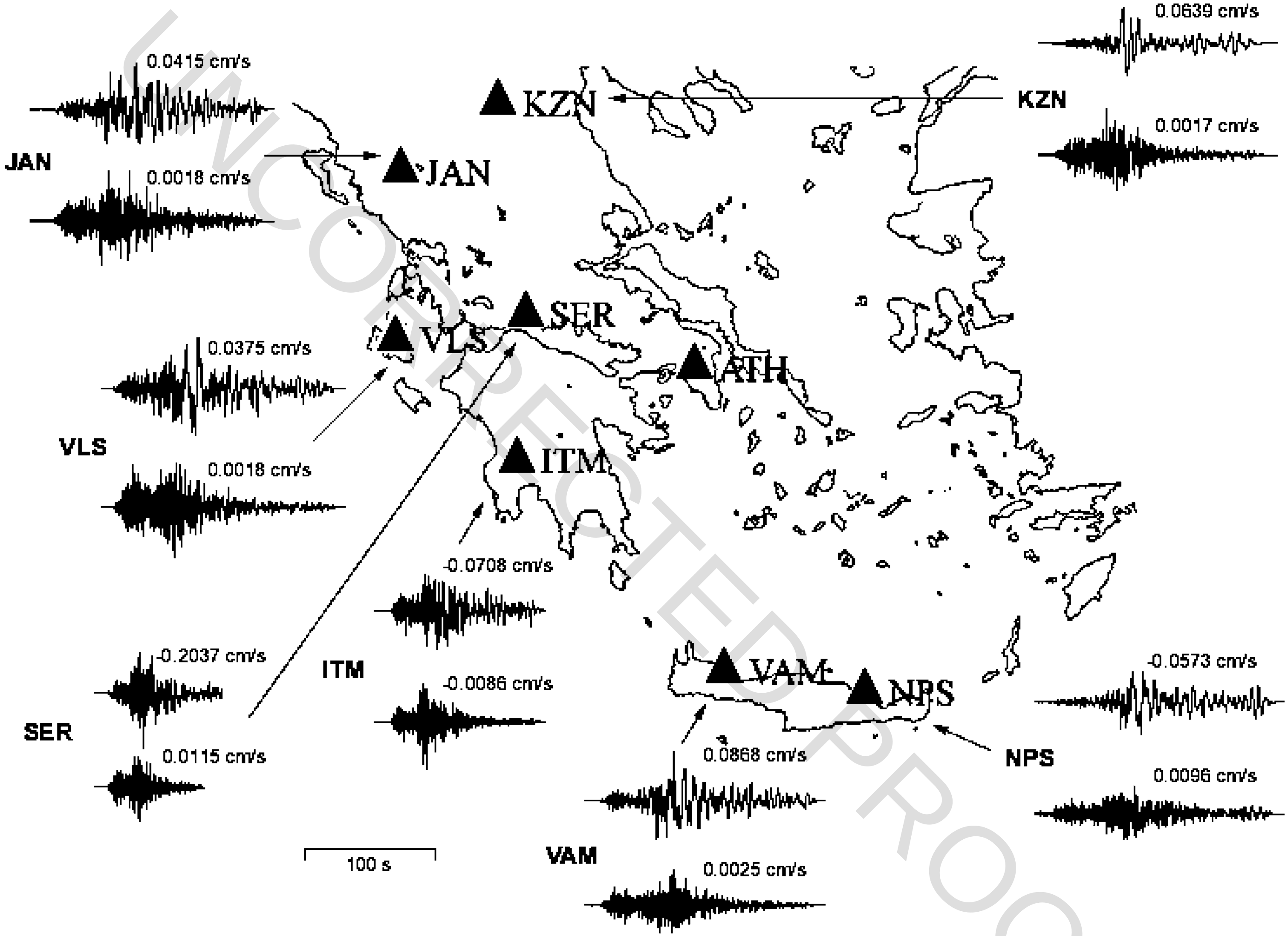

Fig. 1. The velocity records of the Athens mainshock (September 7, 1999, 11:56:50 GMT) (top waveforms) and aftershock (September 8, 1999, 12:55:1 GMT) (bottom waveforms) used in this study. Numbers denote the peak values.

Table 2
Seismic stations used in this study

Station code	Latitude (deg)	Longitude (deg)	Distance (km)	Operated by
SER	38.41N	22.06E	139	Charles University and Patras University
ITM	37.18N	21.93E	184	NOA
VLS	38.18N	20.59E	265	NOA
KZN	40.31N	21.77E	288	NOA
JAN	39.66N	20.85E	292	NOA
VAM	35.41N	24.20E	309	NOA
NPS	35.26N	25.61E	367	NOA

shock are the same. We ask the question whether a special situation exists, in which the eGf method can be applied to earthquakes with nonequal focal mechanisms. The answer is positive if the waveforms corresponding to the different focal mechanisms are very similar, practically unchanged, except a multiplication constant. This may happen at stations, where a single-wave group is dominant, thus we must select a subset of such stations.

To select the stations, we perform the following synthetic test by combining the discrete wave number method (DW) method and the eGf-like summation: we generate finite-extent synthetics for two different focal mechanisms, $a_1(t)$ and $a_2(t)$, that of mainshock and aftershock. These two are compared by computing correlation coefficient and ratio of their peak amplitudes, $R = a_1^{\max}(t)/a_2^{\max}(t)$. The comparison is performed in a time window containing the dominant wave group (see later in Fig. 6) for all stations and for all tested nucleation points. We select the stations characterized by the largest value of the correlation coefficient (averaged over tested nucleation points) and, at the same time, having almost the same correlation coefficient for all nucleation points. The amplitude ratio R at each station is also averaged, in an analogous way, thus providing a station's multiplication constant $\bar{R}$.

Real data from the selected stations are then divided by $\bar{R}$ and inverted using eGf method (Irikura and Kamae, 1994), as if the mainshock and aftershock mechanisms were the same. The goal of the inversion is to find the hypocenter position on the finite fault by the grid search.

At any selected station, the synthetic and observed records are aligned to have the same first onset. For obtaining the shift, the STA/LTA "triggering" algorithm is used with STA = 0.1 s and LTA = 15 s.

The observed and synthetic records are separated into low-frequency (0.0–0.8 Hz) and high-frequency (0.8–20 Hz) parts. The high-frequency part is used to define the "triggering" onset due to sharpness of the first arrival. The low-frequency part is used in

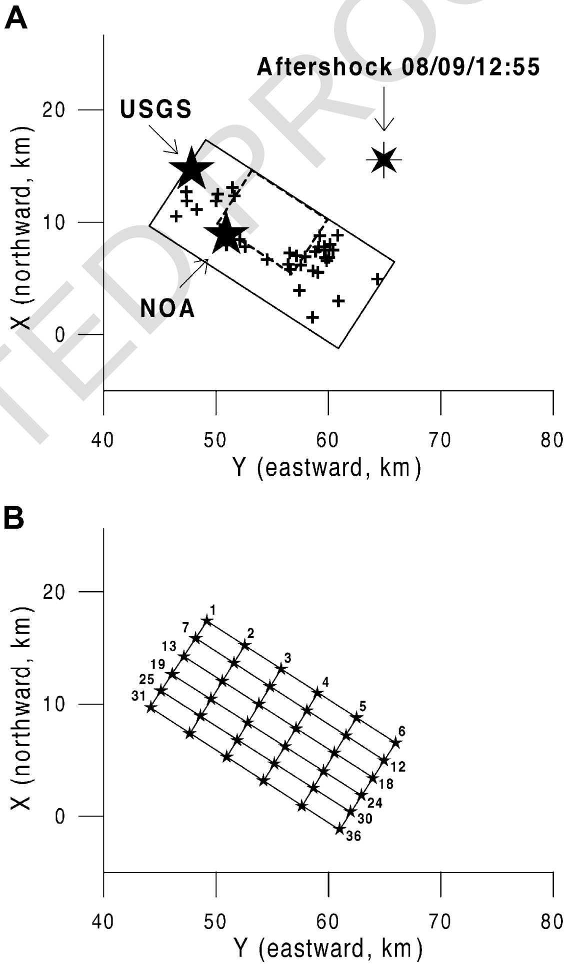

Fig. 2. (A) Epicenters of September 14–25 aftershocks and the inferred fault contours projected onto the Earth surface. A large fault (solid rectangle) and a small fault (dashed rectangle) are considered. The USGS and NOA hypocenters are marked by the stars. The eGf aftershock is shown by the diamond. (B) The large fault plane and 36 tested nucleation points marked by small stars. The analogous numbering is taken for the small fault, not shown here.

the inversion process. The "inverse misfit function" (IMF) is defined as follows:

$$\mathrm{IMF} = \frac{1}{m\sqrt{\sum_{i=1}^{k}\left(\frac{A_i^{\mathrm{synt}}}{A_{\mathrm{max}}^{\mathrm{synt}}} - \frac{A_i^{\mathrm{observed}}}{A_{\mathrm{max}}^{\mathrm{observed}}}\right)^2}},$$

$$m = \begin{cases} \frac{A_{\mathrm{max}}^{\mathrm{observed}}}{A_{\mathrm{max}}^{\mathrm{synt}}}, & \text{for } A_{\mathrm{max}}^{\mathrm{observed}} \geq A_{\mathrm{max}}^{\mathrm{synt}} \\ \frac{A_{\mathrm{max}}^{\mathrm{synt}}}{A_{\mathrm{max}}^{\mathrm{observed}}}, & \text{for } A_{\mathrm{max}}^{\mathrm{observed}} < A_{\mathrm{max}}^{\mathrm{synt}} \end{cases} \tag{1}$$

where $\frac{A_i^{\mathrm{synt}}}{A_{\mathrm{max}}^{\mathrm{synt}}}$ is normalized synthetic time series and $\frac{A_i^{\mathrm{observed}}}{A_{\mathrm{max}}^{\mathrm{observed}}}$ is normalized observed velocity time series. The sum of the squared residuals describes the shape agreement without taking into account the amplitude. The amplitude agreement is quantified by the constant $m \geq 1$. We consider inverse value of the misfit function because of better visualization. The IMF is calculated for the time window given by the synthetic test.

4. Selection of the appropriate stations for Athens earthquake

DW method is used to model synthetic weak events, which will be summed up by the eGf-like method to produce the synthetic mainshock. Their focal mechanisms correspond to the mainshock (strike = 123°, dip = 55°, rake = – 84°) and two known fault-plane solutions of the selected after shock, as discussed above (strike = 220°, dip = 40°, rake = 120°—ASPO and strike = 330°, dip = 70°, rake = – 30°—FMP). Here, ASPO and FMP stand for the amplitude spectra and polarities, and the first motion polarities, respectively. The source time function is a triangle with duration 0.5 s and the scalar seismic moment is 5.2×10^{15} N m.

The finite-extent synthetics are calculated for the large fault plane (20 × 16 km). Its orientation is given by the strike and dip of the mainshock. The rupture is assumed to propagate radially from the hypocenter with constant rupture velocity 3 km/s. We test 36 nucleation points uniformly distributed along the fault plane (Fig. 2B). Two parameters are important for eGf modeling: the stress–drop ratio c (mainshock versus aftershock) and the seismic

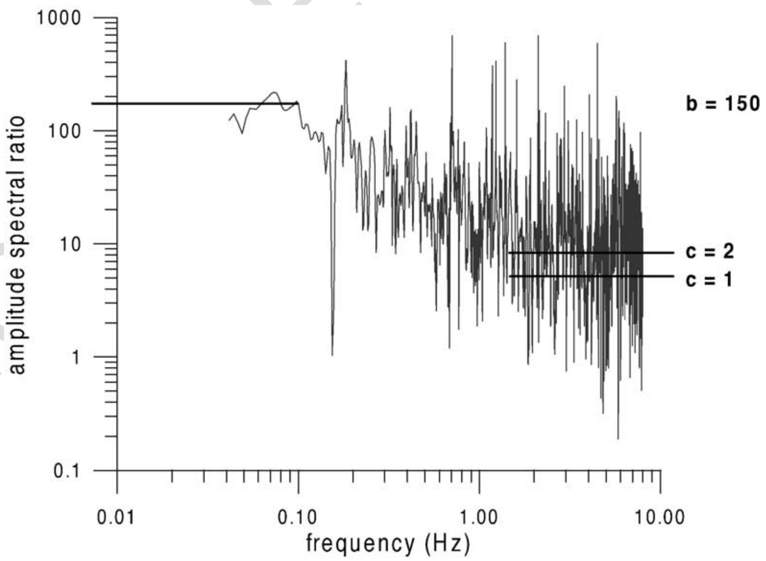

Fig. 3. The amplitude spectral ratio derived from the mainshock and aftershock recorded at SER. Two constants needed in the eGf method, $b = 150$ and $c = 1$ or 2, are fitted to the low- and high-frequency parts.

moment ratio b. We estimate b and c by fitting the low- and high-frequency flat parts of the Fourier amplitude mainshock/aftershock spectral ratio assuming the omega-square model (Lindley, 1994). The parameter $b = 150$ and two values of $c = 1$ or 2 were obtained from real data at the station SER (Fig. 3). For synthetic tests, we adopted the value $c = 1$.

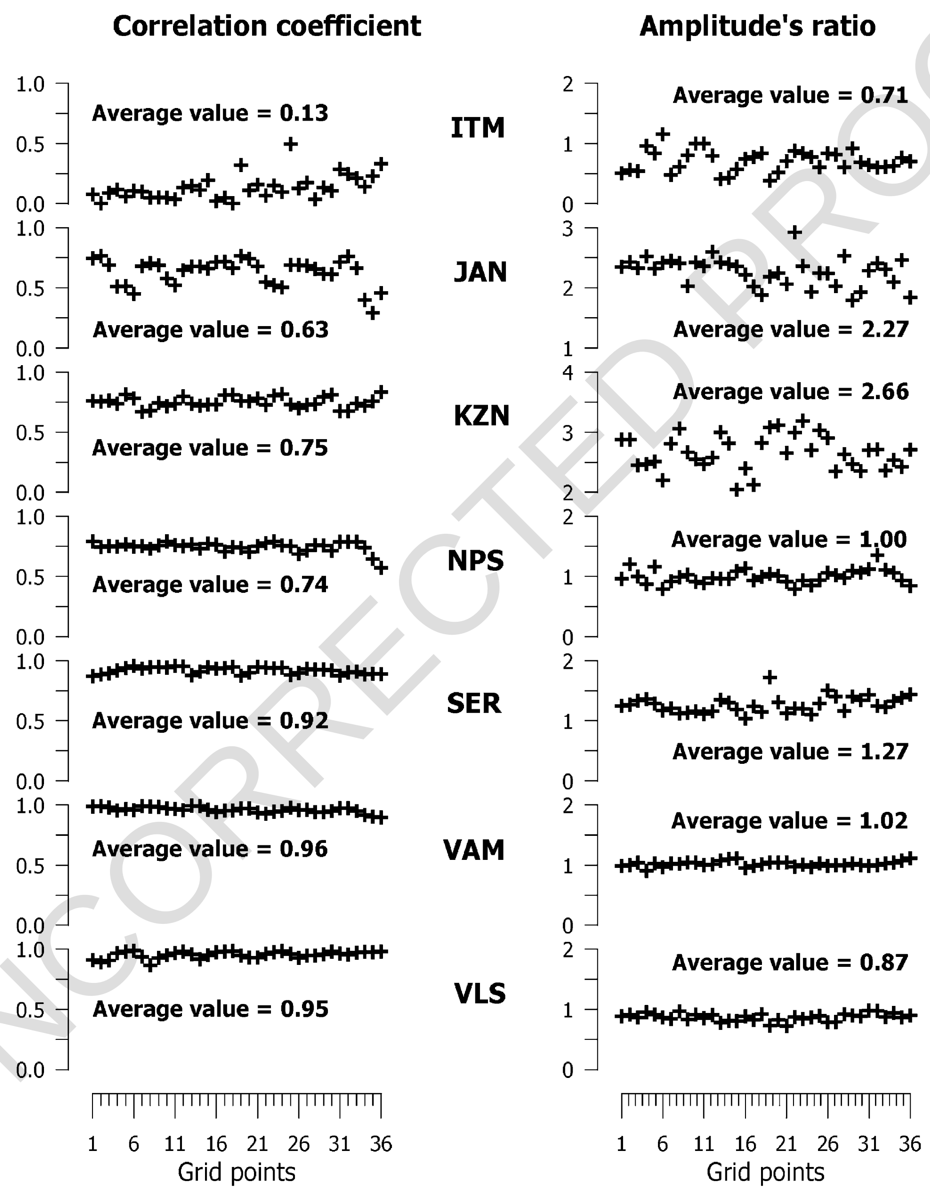

Fig. 4. The correlation coefficients between the mainshock synthetics for two focal mechanisms (mainshock focal mech.: strike = 123°, dip = 55°, rake = – 84° and ASPO focal mech.: strike = 220°, dip = 40°, rake = 120°) and the amplitude ratios shown as a function of the nucleation point. Averages over all nucleation points are also shown.

We perform two independent synthetic experiments:

1. At a station, we compare the finite-extent synthetics for the two focal mechanisms (mainshock and ASPO mechanisms) keeping a common nucleation point (= grid point), and repeat the comparison for all stations and all nucleation points.
2. Same procedure as in experiment 1, but the synthetics computed with ASPO mechanism are replaced by the synthetics computed with FMP mechanism.

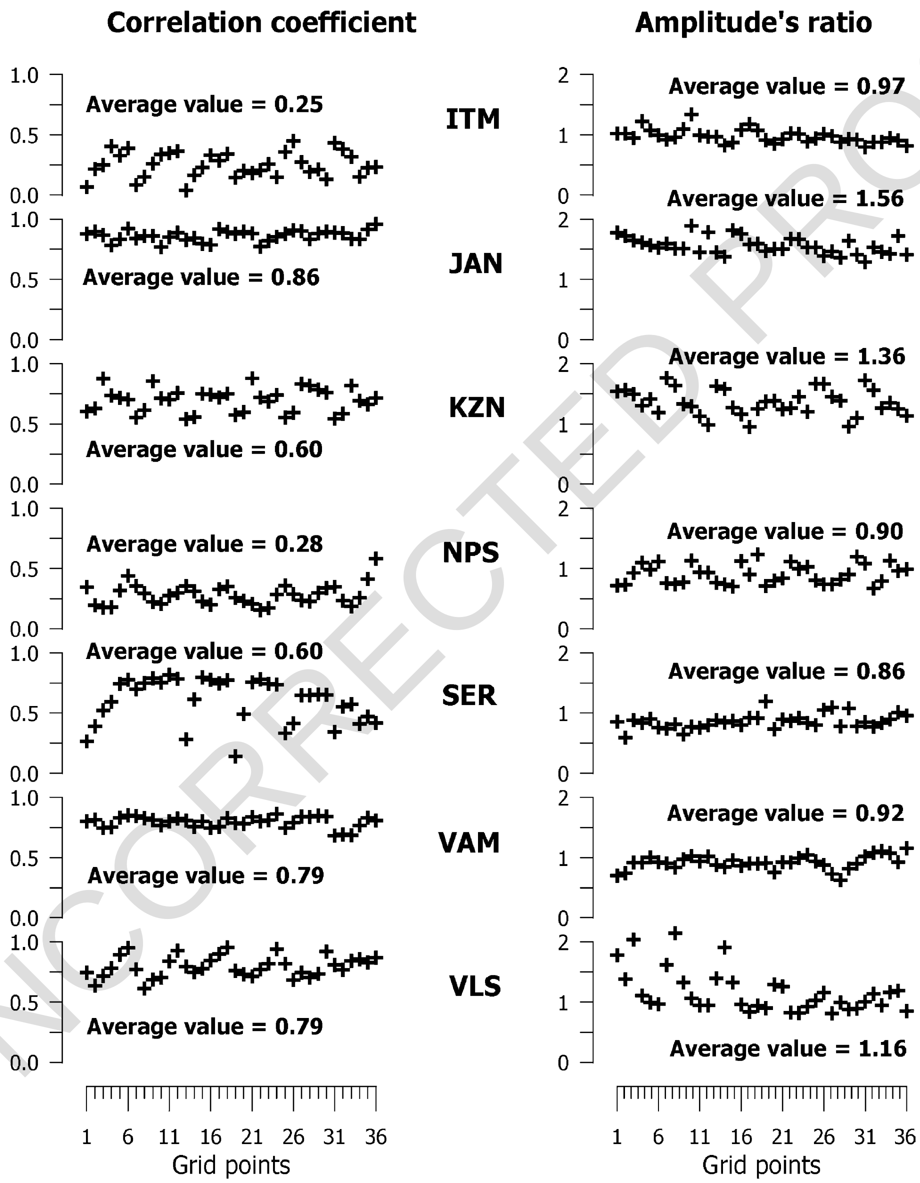

Fig. 5. The correlation coefficients between the mainshock synthetics for two focal mechanisms (mainshock focal mech.: strike = 123°, dip = 55°, rake = – 84° and FMP focal mech.: strike = 330°, dip = 70°, rake = – 30°) and the amplitude ratios shown as a function of the nucleation point. Averages over all nucleation points are also shown.

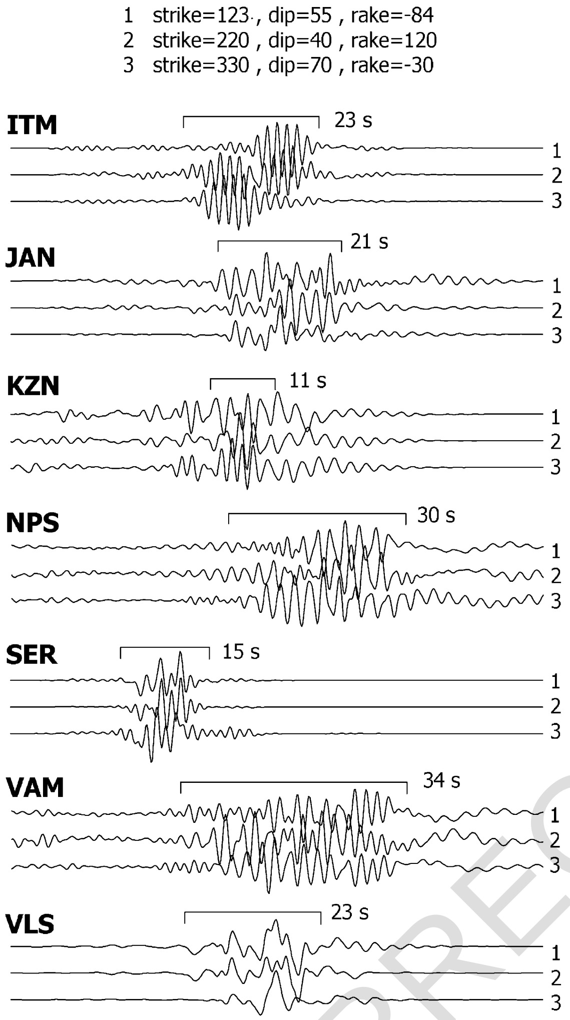

Fig. 6. The comparison of the synthetic mainshocks for three focal mechanisms and for the nucleation points with the lowest value of the correlation coefficient. The horizontal bar shows the time window for which the correlation coefficient is computed.

The correlation coefficients and the amplitude ratios (Figs. 4 and 5) are computed for both experiments as a function of the nucleation points. Their averaged values are also included.

Experiment 1 shows that the different focal mechanisms do not affect the synthetics at stations SER, VAM and VLS, where the values of the correlation coefficient are very high (close to 1) and almost constant for all nucleation points: the amplitude ratio at these stations is close to 1, too. The correlation coefficients at NPS and KZN have lower values than for previous stations, but again, they are nearly constant; the amplitude ratio is very oscillatory for KZN. Stations ITM and JAN show the lowest value of the average correlation coefficient and the highest degree of oscillation.

Experiment 2 gives two stations JAN and VAM, where correlation coefficient is high and constant for all tested nucleation points. It also shows that the agreement is not good for other stations, so they cannot be used.

The comparison of the synthetic mainshocks for the studied mechanisms at the nucleation point with the lowest value of the correlation coefficient is shown in Fig. 6. We choose the lowest correlation coefficient to show that even in the worst case, the differences are not drastic.

The partial conclusion is as follows: if focal mechanism of the selected aftershock determined by ASPO method is a true one, we can invert stations SER, VAM and VLS with multiplicative constants 1.27, 1.02 and 0.87, respectively (experiment 1). In case that the selected aftershock has focal mechanism estimated by FMP method, we can use stations JAN and VAM, with multiplicative constants 1.56 and 0.92 (experiment 2).

5. Inversion of the Athens data set

Separate inversion of the nucleation point position is done for two possible fault sizes, the large (20×16 km) and small (8×10 km) ones (Fig. 2A), both subdivided into the rectangular grid with

Table 3
Parameters of the eGf simulation

	Large fault (20×16 km)		Small fault (8×10 km)	
	$c=1$	$c=2$	$c=1$	$c=2$
$N \times N$	5×5	4×4	5×5	4×4
$l \times w$ (km)	4×2	5×2.5	1.6×3.2	2×4

c = Stress/drop ratio mainshock versus aftershock, N = number of subfaults along strike and dip, l and w = subfault length along strike and dip.

36 examined nucleation points (Fig. 2B). We use the parameters presented in Table 3. We tested values of the rise time *T*, ranging from 0.1 to 1 s, and found the most appropriate value 0.27 s.

We now apply the method described in the previous sections. Fig. 7 shows the inverse misfit functions (corrected at each station for different focal mechanisms) for the first subset of the stations (VAM, VLS and SER) (experiment 1). Fig. 8 is for the second subset (JAN, VAM) (experiment 2). Results for large and small faults are shown. The highest value of the IMF (the highest column) denotes the nucleation point with the best agreement between the observed and synthetic data. Resolution for the large fault is better than for the small one. This can be explained by the fact that with finer grid on the small fault, the waveform changes due to a varying nucleation point are weaker.

For all best-fitting nucleation points, we found very good agreement between the observed and synthetic seismograms for all selected stations and both fault sizes (Fig. 9).

The first subset of the selected stations (VAM, VLS and SER), corresponding to experiment 1, assuming the ASPO mechanism, provided the possible nucleation point at grid points shown in Fig. 10 by diamonds. The second subset of the stations (JAN and VAM), experiment 2, assuming the FMP mechanism, provided the nucleation-point positions shown in Fig. 10 by stars. The results of the inversions for both station subsets (experiments 1 and 2) are compatible because both indicate the nucleation point at the western edge of the fault.

The comparison between the observed and synthetic data is performed on the low-pass (0 to 0.8 Hz) filtered records for JAN, VAM and VLS. The closest station

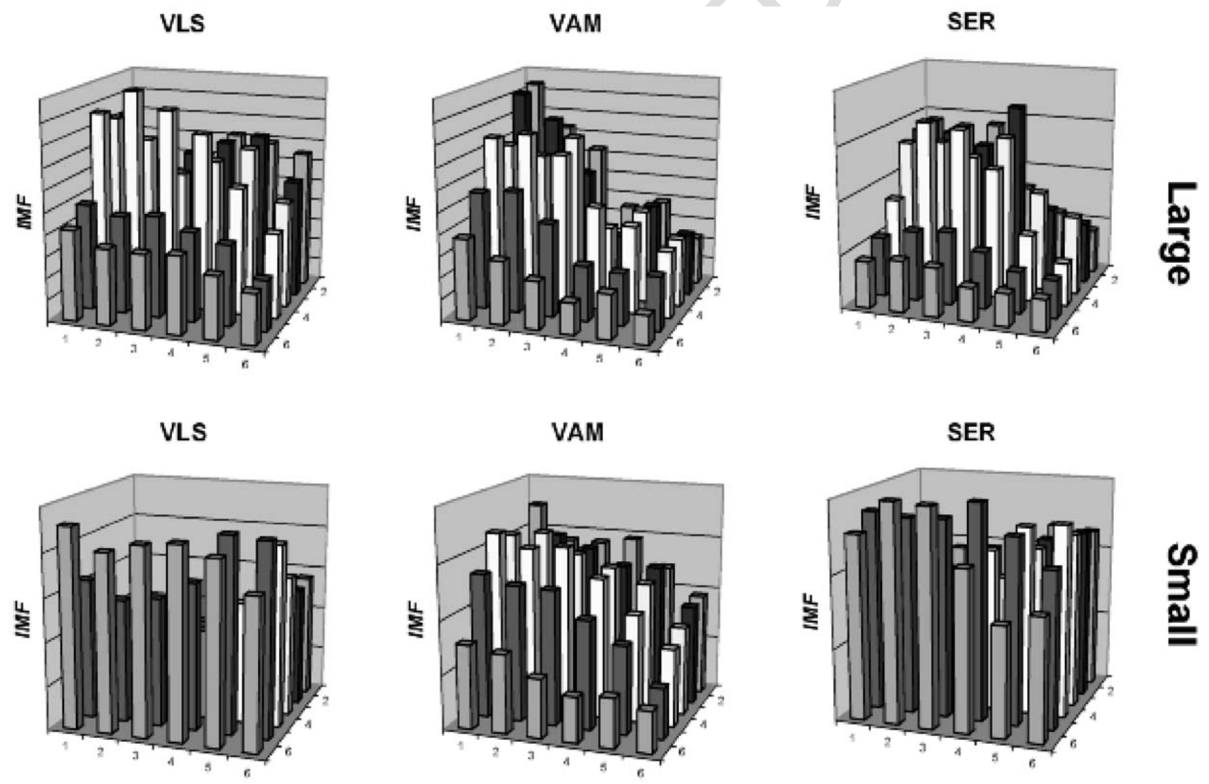

Fig. 7. The inverse misfit function (IMF) computed from waveforms at stations VAM, VLS and SER for the large (top) and small (bottom) faults. The likely hypocenter position is that of the largest column. The base of each plot is the fault plane. Shading is used to improve the identification of the individual grid lines (ASPO focal mechanism).

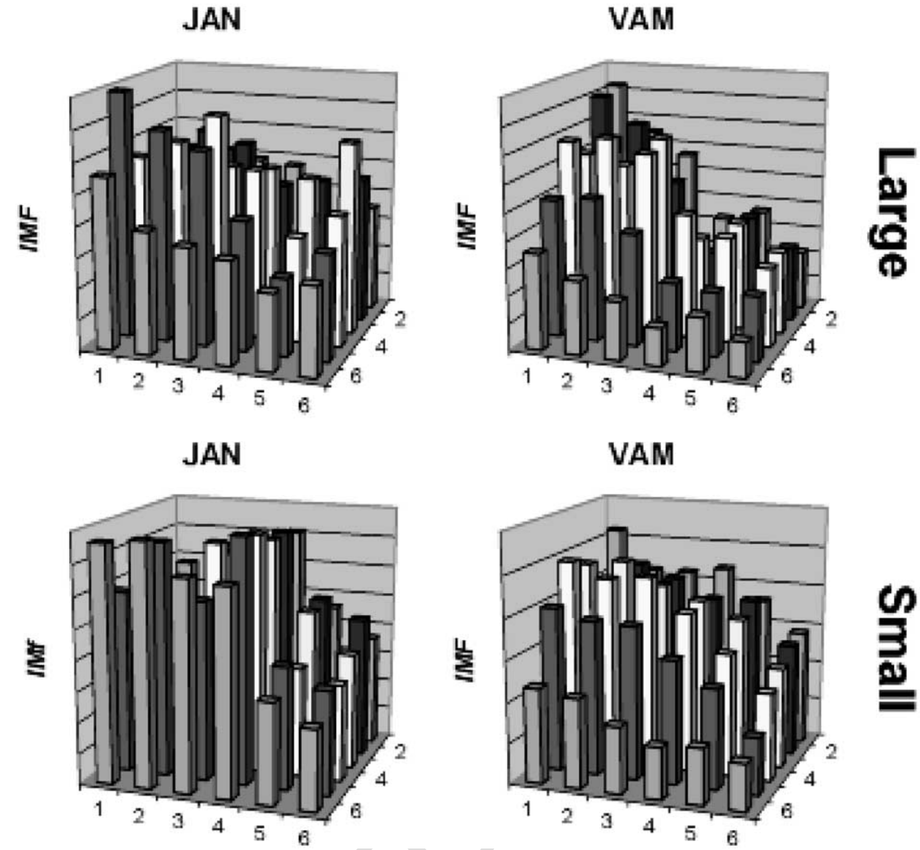

Fig. 8. The inverse misfit function (IMF) computed from waveforms at stations JAN and VAM for the large (top) and small (bottom) faults. The likely hypocenter position is that of the largest column. The base of each plot is the fault plane. Shading is used to improve the identification of the individual grid lines (FMP focal mechanism).

SER is filtered more (0 to 0.3 Hz) because the records at the station are complex.

6. Inversion with another aftershock

We tried also to use an aftershock ($M_L = 3.7$, September 8, 1999, 03:35 GMT, Lat. = 38.12N, Lon. = 23.89E, NOA) whose focal mechanism is very similar to the mainshock, as found from the first-motion polarities (Papadopoulos et al., 2000). Anyway, usage of that weak earthquake as eGf is difficult due to lower signal-to-noise ratio (Fig. 11). Therefore, the agreement between observed and simulated records is very poor (Fig. 12). The event does not contribute to this study except further emphasizing importance of aftershocks with good signal-to-noise ratio. No aftershock of a better quality compared to that one discussed in the preceding sections is available.

7. Discussion

The previous results were obtained for the fixed position and orientation (strike = 123°, dip = 55°) of the mainshock fault plane. A question of how sensitive the method is with respect to knowledge of the fault plane arises. This question is addressed by an additional synthetic test, using station KZN.

We assume the nucleation point 31 on the studied plane (strike = 123°, dip = 55°), and generate the eGf synthetics for KZN. Then we invert such KZN

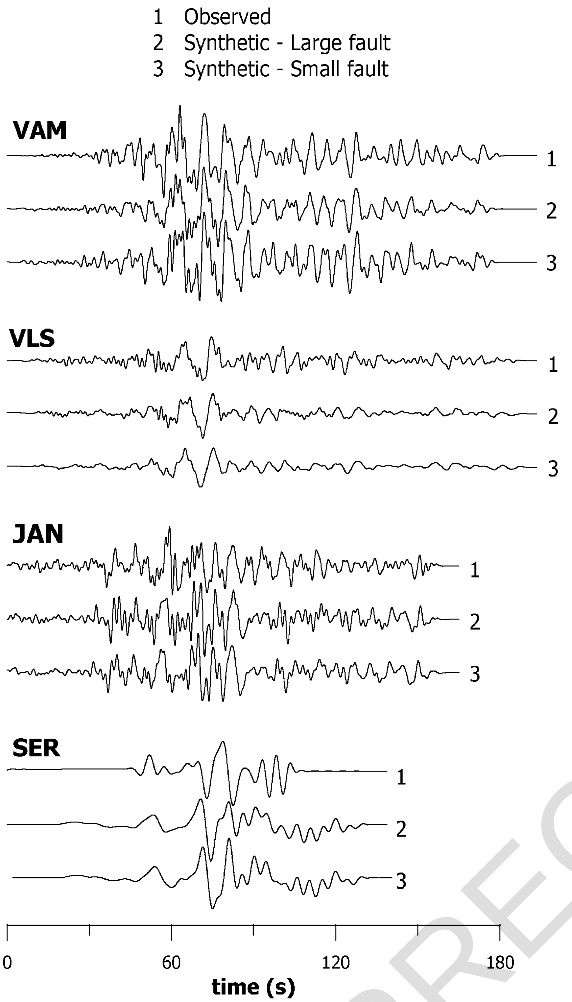

Fig. 9. Comparison between observed (1) and best-fitting eGf synthetic data for large (2) and small (3) faults at stations VAM, VLS, JAN and SER.

artificial record in three ways: (A) at the same plane (strike = 123°, dip = 55°), (B) at the conjugate nodal plane (strike = 292°, dip = 36°) and (C) at an arbitrarily chosen plane (strike = 213°, dip = 55°). The aftershock employed in tests A, B and C remains the same. As expected, A correctly returns the nucleation point 31. Note that the value of the IMF at point 31 is infinity, but it is plotted as a large finite value.

Cases B and C provide completely different and wrong nucleation point, not 31. For example, choosing the second nodal plane (case B) yields IMF resembling a mirror image of that in Fig. 13A. At the same time, the agreement between the synthetics and "data" in Fig. 14 is still very good.

We thus arrive to an important warning that quality of the fit between synthetic and observed waveforms is not sufficient for measuring the success of an inversion. A false agreement may exist for improper fault orientation, which, in fact, may result in a completely wrong conclusion about the rupture propagation. However, because the Athens earthquake fault plane has been well con-

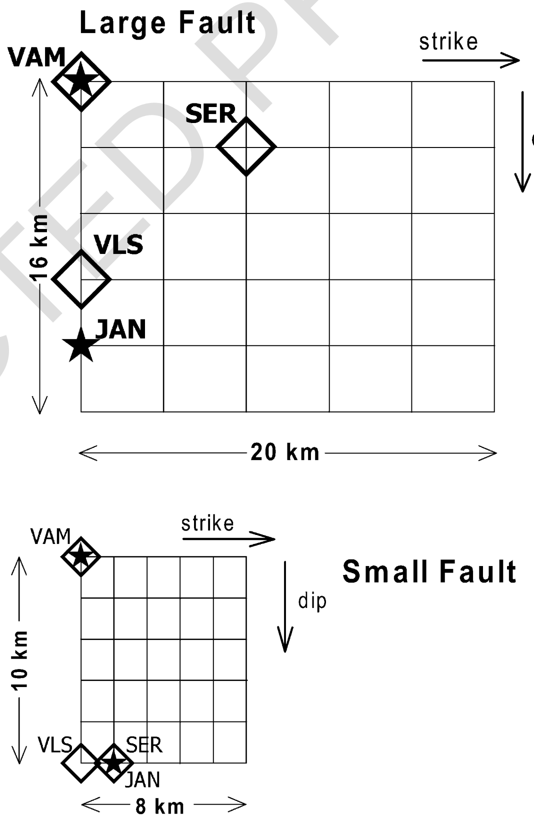

Fig. 10. Grid of the 36 tested hypocenters projected onto the earth surface for the large (top) and small (bottom) faults. The symbols denote the best-fitting positions of the nucleation point obtained from the indicated stations. The diamonds show the nucleation points obtained with consideration of the ASPO focal mechanisms (strike = 220°, dip = 40°, rake = 120°). The stars show the nucleation points obtained with consideration of the FMP focal mechanisms (strike = 330°, dip = 70°, rake = – 30°).

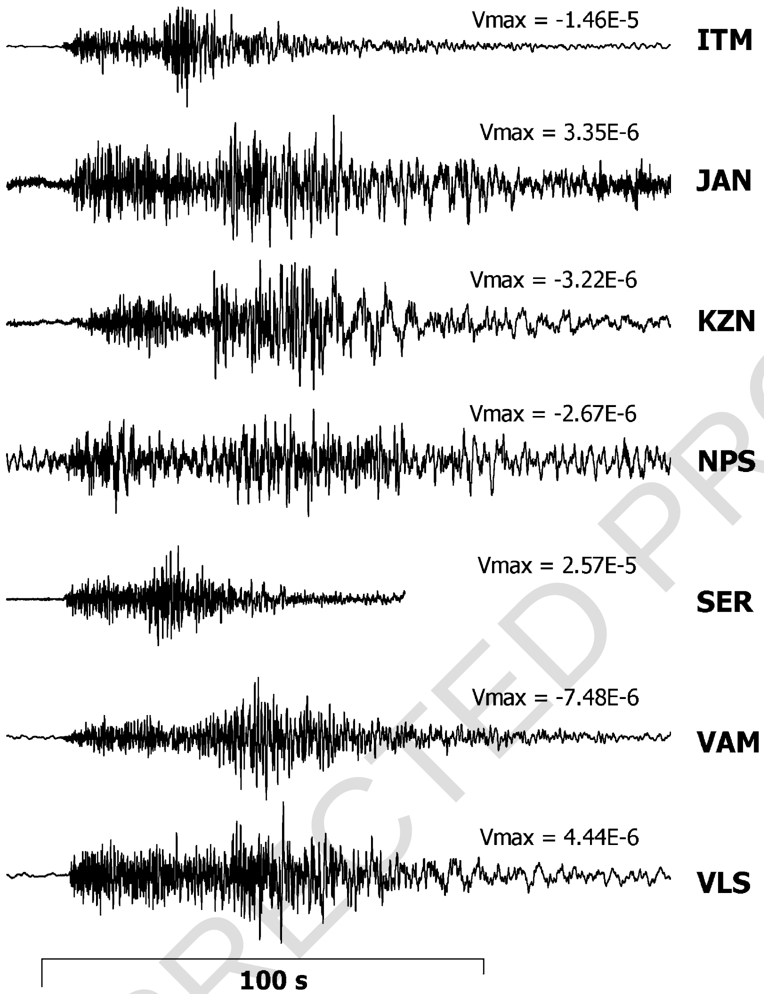

Fig. 11. The E–W components of the aftershock (M_L = 3.7, September 8, 1999, 03:35 GMT, Lat. = 38.12N, Lon. = 23.89E, NOA) at stations ITM, JAN, KZN, NPS, SER, VAM and VLS whose focal mechanism (strike = 106°, dip = 30°, rake = – 74°; Papadopoulos et al., 2000) is similar to the one of the mainshock.

firmed by aftershocks, we can trust the results of Fig. 10.

We conclude that eGf inversion is possible for mainshock and aftershock of unequal (known) focal mechanisms, provided that a suitable station subset and multiplicative constants are found by synthetic experiments. In the case of Athens earthquake, two focal mechanisms are known for the selected aftershock; therefore, we use two station subsets, in two separate experiments (SER, VAM, VLS in experiment 1, and JAN, VAM in experiment 2). Both inversions reveal the nucleation point to be at the left-hand (western) part of the fault plane, thus suggesting east rupture propagation toward Athens. Directivity effect was independently confirmed by Sargeant et al. (2000) using teleseismic data. Papadopoulos et al. (2000) and Papadimitriou et al. (2000) also propose rupture propagation from west to east based on the observation that four foreshocks occurred west of the mainshock. The fault sizes of our paper are in rough agreement with Wells and Coppersmith (1994), Papazachos and Papazachou (1997), Somerville et al. (1999), Papadimitriou

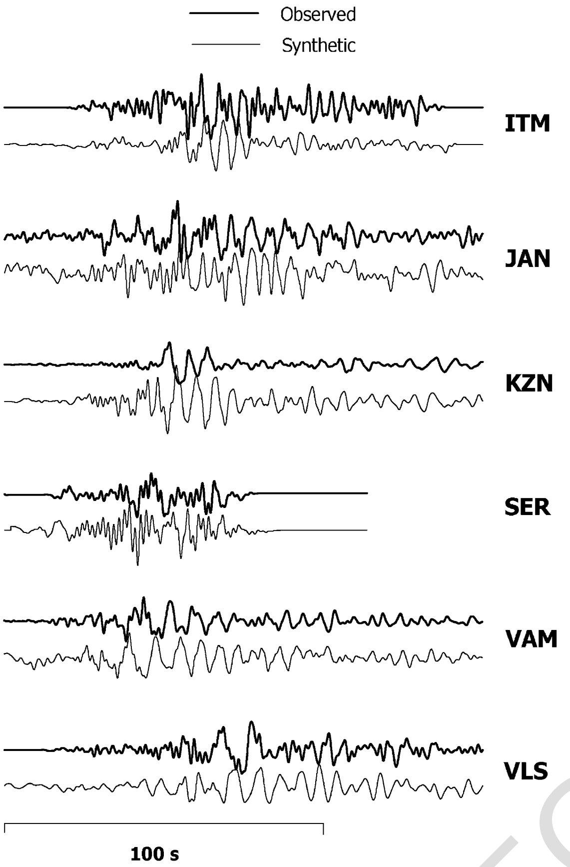

Fig. 12. Comparison between observed and best-fitting eGf synthetic data for large fault at stations ITM, JAN, KZN, SER, VAM and VLS for aftershock (Fig. 11) with the similar focal mechanism as mainshock. The station NPS is not used in inversion due to very low signal-to-noise ratio.

et al. (2000) and Sargeant et al. (2000). Tselentis and Zahradnik (2000) have shown that the duration of the source time function is about 5–6 s at regional stations, which is also consistent with the range of fault dimensions considered here.

8. Conclusion

The classical empirical Green's function method has been innovated to allow unequal focal mechanisms of the mainshock and aftershock. The method was used to invert regional records of the 1999 Athens

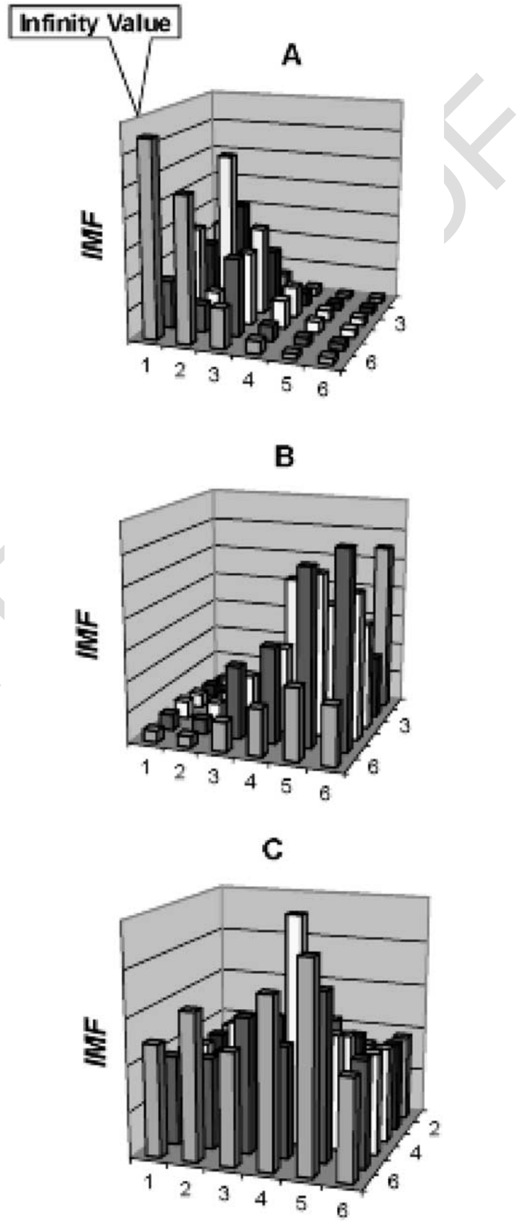

Fig. 13. The synthetic tests at KZN station aimed to retrieve a given nucleation point 31 on a "true" fault plane with strike = 123° and dip = 55°. (A) Inversion in which correct fault-plane orientation is assumed (strike = 123°, dip = 55°); (B) inversion with a fault plane conjugated with respect to the true one (strike = 292°, dip = 36°); (C) inversion with an arbitrary chosen fault-plane orientation (strike = 213°, dip = 55°).

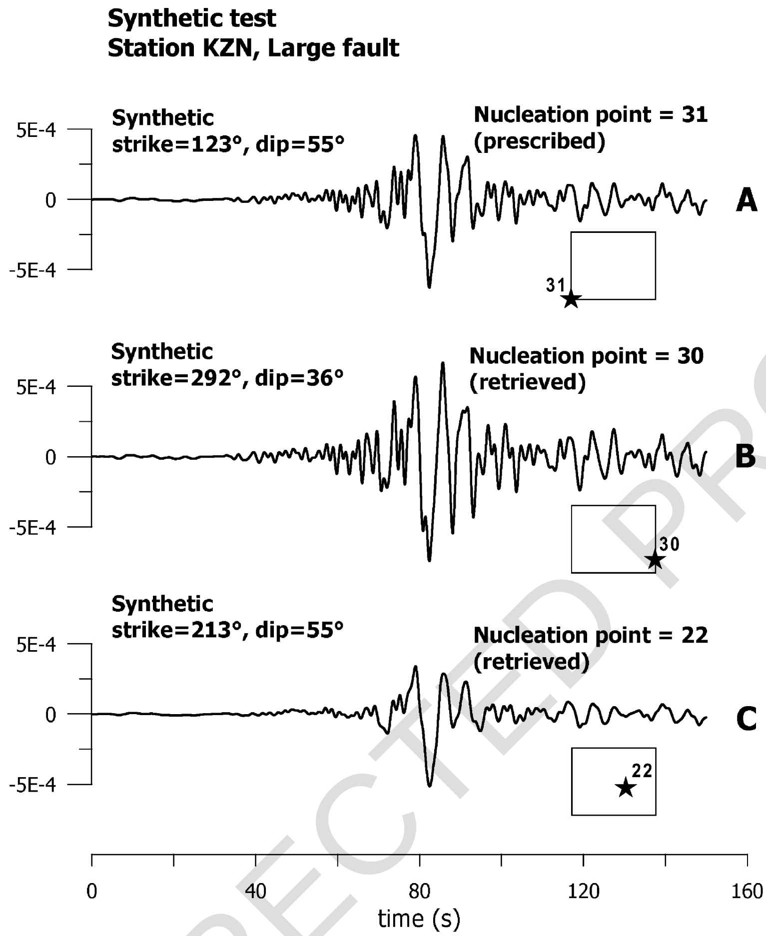

Fig. 14. Comparison between synthetic record (A) and two best-fitting records for two different inversions with wrong orientation of the fault plane (B and C). Cases B and C retrieve wrong nucleation points. See also Fig. 13.

earthquake for position of the nucleation point on the fault plane known for the aftershock distribution. Eastward rupture propagation was found.

Acknowledgements

The authors thank the National Observatory of Athens for their records. The long-lasting cooperation with the Seismological Laboratory of the Patras University has been possible; thanks to G.-Akis Tselentis. The authors also thank Jaromir Jansky for his careful reading of the manuscript. The constructive reviews of Susan E. Hough, Giseppe De Natale, C. Trifu and Hans Thybo improved the paper. Financial support from the following sources is highly appreciated: NATO Collaborative Linkage grant EST.CLG.976035; EC project EVG1-CT-1999-00001 PRESAP; and several research projects in the Czech Republic, MSMT J13/98-113200004, ME354, GAUK 176/2000 and GACR 205/00/0902.

References

Diagourtas, D., Makropoulos, K.C., Wajeman, C., Hatzfeld, D., Bard, P.-Y., Gariel, J.-C., 1994. Simulation of strong ground motion of the July 1993 Patras earthquake and its contribution in the assessment of seismic hazard, Patras region, W. Greece. In: Makropoulos, C., Suhadolc, P. (Eds.), Proc. of ESC XXIV

General Assembly, Athens, Greece, 19–24 September 1994, pp. 1446–1454.

Dreger, D.S., 1994. Empirical Green's function study of the January 17, 1994 Northridge, California earthquake. Geophys. Res. Lett. 21, 2633–2636.

Frankel, A., 1995. Simulating strong motions of large earthquakes using recordings of small earthquakes: the Loma Prieta mainshock as a test case. Bull. Seismol. Am. 85, 1144–1160.

Hartzell, S.H., 1978. Earthquake aftershocks as Green's functions. Geophys. Res. Lett. 5, 1–4.

Hough, S.E., 2001. Empirical Green's function analysis of recent moderate events in California. Bull. Seismol. Am. 91, 456–467.

Hutchings, L., Wu, F.T., Jarpe, S., Kasameyer, P., Foxal, W., Ioannidou, E., Stavrakakis, G.N., 1997. Strong ground motion synthesis for earthquakes in the Gulf of Corinth using empirical Green's function. The 29th General Assembly of the IASPEI, Thessaloniki, Greece, 18–28 August 1997.

Irikura, K., Kamae, K., 1994. Estimation of strong motion in broadfrequency band based on a seismic source scaling model and an empirical Green's function technique. Ann. Geofis. XXXVII, 1721–1743.

Lindley, G.T., 1994. Source parameters of the 23 April 1992 Joshua Tree, California, earthquake, its largest foreshock, and aftershocks. Bull. Seismol. Soc. Am. 84, 1051–1057.

Papadimitriou, P., Kaviris, G., Voulgaris, N., Kassaras, I., Delibasis, N., Makropoulos, K., 2000. The September 7, 1999 Athens earthquake sequence recorded by the Cornet network: preliminary results of source parameters determination of the mainshock. Ann. Geol. Pays Hell. 38 (ser. 1, fasc. B), 29–39.

Papadopoulos, G.A., Drakatos, G., Papanastassiou, D., Kalogeras, I., Stavrakakis, G., 2000. Preliminary results about the catastrophic earthquake of 7 September 1999 in Athens, Greece. Seismol. Res. Lett. 71, 318–329 (see also erratum, vol. 72, p. 76).

Papanastassiou, D., Stavrakakis, G.N., Drakatos, G., Papadopoulos, G., 2000. The Athens, September 7, 1999, Ms = 5.9, earthquake: first results on the focal properties of the main shock and the aftershock sequence. Ann. Geol. Pays Hell. 38 (ser. 1, fasc. B), 73–88.

Papazachos, B.C., Papazachou, C., 1997. The Earthquakes of Greece. Ziti Publ., p. 356.

Plicka, V., Zahradnik, J., 1998. Inverting seismograms of weak events for empirical Green's tensor derivatives. Geophys. J. 132, 471–478.

Sargeant, S.L., Burton, P.W., Douglas, A., Evans, J.R., 2000. A source model for the 7th September 1999 Athens earthquake. Proceedings of the 27th Gen. Ass. of the Europ. Seismol. Comm., Lisbon 10–15 Sep. 2000.

Somerville, P., Irikura, K., Graves, R., Sawada, S., Wald, D., Abrahamson, N., Kagava, Y.I.T., Smith, N., Kowada, A., 1999. Characterizing crustal earthquake slip models for the prediction of strong ground motion. Seismol. Res. Lett. 70, 59–80.

Stavrakakis, G.N., Chouliaras, G., Panopoulou, G., 2000. Seismic source parameters for the Athens earthquake on September 7, 1999, from a new telemetric broad band seismological network in Greece. Ann. Geol. Pays Hell. 38 (ser. 1, fasc. B), 15–28.

Tselentis, G.-A., Zahradnik, J., 2000. The Athens earthquake of September 7, 1999. Bull. Seismol. Soc. Am. 90, 1143–1160.

Wells, D.L., Coppersmith, K.J., 1994. New empirical relationships among magnitude, rupture length, rupture width, rupture area, and surface displacement. Bull. Seismol. Soc. Am. 84, 974–1002.

Zahradnik, J., 2001. Focal mechanism of the Athens 1999 earthquake by ASPO method, Research report, Dept. of Geophysics, Charles University, Prague (see also http://seis30.karlov.mff.cuni.cz).